Available online at www.sciencedirect.com
SCIENCE DIRECT®
Journal of Solid State Chemistry 177 (2004) 739–744
JOURNAL OF SOLID STATE CHEMISTRY
http://elsevier.com/locate/jssc

Crystal structures, magnetic and thermal properties of Ln_3IrO_7 (Ln = Pr, Nd, Sm, and Eu)

Hiroaki Nishimine,* Makoto Wakeshima, and Yukio Hinatsu

Graduate School of Science, Division of Chemistry, Hokkaido University, Kita 10-Jo, Nishi 8-Chome, Sapporo 060-0810, Japan

Received 21 April 2003; received in revised form 10 July 2003; accepted 24 August 2003

Abstract

Ternary iridium oxides Ln_3IrO_7 (Ln= Pr, Nd, Sm, and Eu) were prepared and their crystal structures, magnetic and thermal properties were investigated. Powder X-ray diffractions (XRDs) were measured for all samples and neutron diffraction (ND) measurements were performed for Pr_3IrO_7. All the profiles were refined with space group *Cmcm* (No. 63). The lattice parameters for Pr_3IrO_7 refined by using ND data are $a = 10.9782(13)$ Å, $b = 7.4389(9)$ Å, and $c = 7.5361(9)$ Å. From specific heat and differential thermal analysis (DTA) measurements, Ln_3IrO_7 (Ln= Pr, Nd, Sm, and Eu) show thermal anomalies at 261, 342, 420, and 485 K, respectively. The results of powder high-temperature XRD and ND measurements indicate that these anomalies are due to the structural phase transition. Magnetic susceptibilities of these compounds were measured in the temperature range between 1.8 and 400 K. Nd_3IrO_7 shows an antiferromagnetic transition at 2.6 K. A specific heat anomaly has also been observed at the same temperature. For Ln_3IrO_7 (Ln= Pr, Sm, and Eu), no magnetic anomalies have been found in the experimental temperature range.

Keywords: Lanthanide; Iridium; Structural phase transition; Antiferromagnetic transition; Magnetic susceptibility; Specific heat

1. Introduction

Ternary iridium compounds Ln_3IrO_7 (Ln= Pr, Nd, Sm, and Eu) are members of a large family of chain compounds Ln_3MO_7 (Ln = rare-earth metals, M = pen- = pentavalent 4*d*, 5*d* transition metals). Since Rossell et al. [1,2] determined the parent structure of this family, La_3NbO_7, the crystal structure and physical properties of Ln_3MO_7 compounds containing a variety of M cations (M= Nb, Mo, Ru, Ta, Re, Os, and Ir) have been investigated [3–19]. The M^{5+} cation is coordinated with six oxygen ions and they form an MO_6 octahedron. These octahedra share corners forming a zigzag chain. The interchain $M-M$ distance is about 6.6 Å compared with the corresponding intrachain distance of 3.7 Å, which suggests that these compounds may exhibit one-dimensional electronic behavior. Most of the rare-earth metals, however, have a nonzero spin, which could lead to long-range order at some finite temperatures due to $Ln-M$ coupling.

Among members of this family, magnetic and electronic properties of ruthenium-based oxides Ln_3RuO_7 (Ln= La, Pr, Nd, and Sm–Gd) have been studied extensively [4,10–16]. They show structural phase transitions and interesting magnetic behavior at low temperatures [14–16]. We have concentrated our attention on the corresponding ternary iridium oxides Ln_3IrO_7, because these iridium compounds may also have many attractive physical properties as the ruthenium compounds. Vente et al. [5,6] synthesized the Ln_3IrO_7 (Ln= Pr, Nd, Sm, and Eu) for the first time.

In this paper, we will report the synthesis, crystal structures, magnetic and thermal properties of Ln_3IrO_7 (Ln= Pr, Nd, Sm, and Eu). Their magnetic and thermal properties have been investigated by the measurements of the magnetic susceptibility, specific heat, differential thermal analysis (DTA), high-temperature X-ray diffraction (XRD), and neutron diffraction (ND).

2. Experimental

Polycrystalline samples of Ln_3IrO_7 (Ln= Pr, Nd, Sm, and Eu) were synthesized by a solid-state reaction. As starting materials, lanthanide oxides Pr_6O_{11} and Ln_2O_3 (Ln= Nd, Sm, and Eu) and iridium metal powders Ir (in all cases, the purity was more than 99.9%) were used.

*Corresponding author. Fax: +81-11-746-2557.
E-mail address: nishi@sci.hokudai.ac.jp (H. Nishimine).

0022-4596/$ - see front matter © 2003 Elsevier Inc. All rights reserved.
doi:10.1016/j.jssc.2003.08.036

They were weighed in an appropriate metal ratio and well mixed in an agate mortar. The mixtures were pressed into pellets and then heated in an oxygen atmosphere up to 1200–1250°C at a rate of 0.5°C min^{-1}, held at this temperature for 12 h, and then cooled down to room temperature at the same rate. After regrinding and repelleting, this heating procedure was repeated again. The heating in an oxygen atmosphere was necessary to avoid the formation of pyrochlore-type compounds $Ln_2Ir_2O_7$ (*Ln*= Pr, Nd, Sm, and Eu) in which the Ir^{4+} ions are present.

Powder XRD profiles for all the samples were measured with Cu*K*α radiation on a MultiFlex diffractometer (Rigaku) at room temperature. The XRD data were collected by the step scanning over the 2θ range of 10–120° at intervals of 0.02°. For Nd_3IrO_7, high-temperature XRD measurements were also performed over the temperature range of 300–500 K. The sample of Nd_3IrO_7 was mounted on the aluminum sample holder. The heater was equipped with the sample holder and the measurements were carried out under the same condition as those at room temperature. Powder ND profiles for Pr_3IrO_7 were measured at 250 K and room temperature. The measurements were performed on the Kinken powder neutron diffractometer with high efficiency and high resolution, HERMES, of the Institute for Materials Research, Tohoku University, installed at the JRR-3M Reactor in the Japan Atomic Energy Research Institute, Tokai [20]. In all cases, the crystal structures were determined by the Rietveld technique, using the program RIETAN 2000 [21].

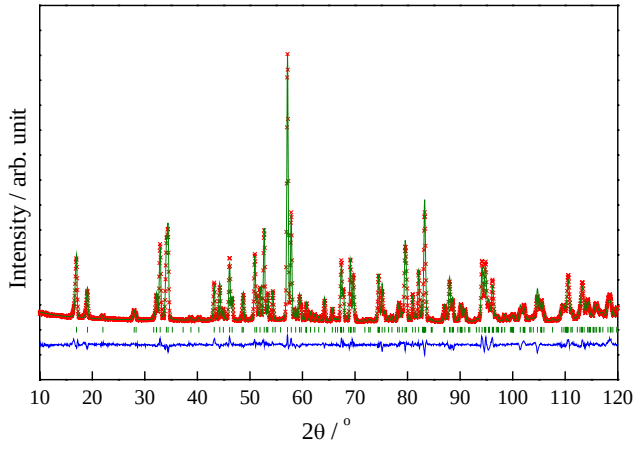

Fig. 1. Powder ND profiles for Pr_3IrO_7. The calculated and observed diffraction profiles are shown on the top as a solid line and cross markers, respectively. The vertical markers show positions calculated from Bragg reflections. The bottom trace is a plot of the difference between the calculated and observed intensities.

Magnetic susceptibility measurements were performed with a SQUID magnetometer (Quantum Design, MPMS model). The temperature dependence of the magnetic susceptibilities was measured under both zero-field-cooled (ZFC) and field-cooled (FC) conditions in an applied field of 0.1 T over the temperature range of 1.8–400 K.

Specific heat measurements for Ln_3IrO_7 (*Ln*= Pr, Nd, and Sm) were performed using a relaxation technique with a heat capacity measurement system (Quantum Design, PPMS model) over the temperature range of 1.8–400 K. The sintered samples were mounted on a thin alumina plate with grease for better thermal contact. DTA measurements for Sm_3IrO_7 and Eu_3IrO_7 were performed with a TG-DTA 2000S (Mac Science) over the temperature range of 300–800 K. As a standard material, α-Al_2O_3 was used and the rates of heating and cooling were both controlled at 10°C min^{-1}.

3. Results and discussion

3.1. Crystal structures

In order to determine the crystal structures, the XRD data for all the samples and the ND data for Pr_3IrO_7 were refined by the Rietveld method. The ND profiles for Pr_3IrO_7 are shown in Fig. 1. Vente et al. [5,6] reported that the crystal structures for Ln_3IrO_7 (*Ln*= Pr, Nd, Sm, and Eu) were orthorhombic with space group *Cmcm*. Following them, we also tried to refine the structures with the same space group for all the diffraction data. Table 1 lists the crystal structure data for Pr_3IrO_7 refined by using ND data at room

Table 1
Crystal structure data for Pr_3IrO_7 at room temperature from powder neutron diffraction

Atom	Position	*x*	*y*	*z*	*B*(Å^2)
Space group *Cmcm* (No. 63), $Z = 4$, $a = 10.9782(13)$ Å, $b = 7.4389(9)$ Å, $c = 7.5361(9)$ Å, $V = 615.4(1)$ Å^3, $R_{WP} = 6.66\%$, $R_I = 2.74\%$, $S = 1.35$					
Pr (1)	4*a*	0	0	0	0.93(8)
Pr (2)	8*g*	0.2222(2)	0.3083(3)	1/4	0.66(6)
Ir	4*b*	0	1/2	0	0.47(4)
O (1)	16*h*	0.1256(1)	0.3171(2)	0.9582(2)	1.08(4)
O (2)	8*g*	0.1308(2)	0.0289(3)	1/4	0.56(5)
O (3)	4*c*	0	0.4098(4)	1/4	0.41(6)

Note: Definitions of reliability factors R_{WP} and R_I are given as follows: $R_{WP} = \left[\sum w(|F_o| - |F_c|)^2 / \sum w|F_o|^2\right]^{1/2}$ and $R_I = \sum|I_{ko} - I_{kc}| / \sum I_{ko}$.

temperature. Fig. 2 shows the crystal structure for Pr_3IrO_7.

Fig. 3 shows the variation of lattice parameters for Ln_3IrO_7 (Ln= Pr, Nd, Sm, and Eu) with the Ln^{3+} ionic radius in eight coordination [22]. The lattice parameters a and c increase monotonously with Ln^{3+} ionic radius from Eu^{3+} to Pr^{3+}. The lattice parameter b also increases monotonously from Eu^{3+} to Nd^{3+}, but decreases from Nd^{3+} to Pr^{3+}. This results indicates that the structure of Pr_3IrO_7 is different from those of all the other compounds Ln_3IrO_7 (Ln= Nd, Sm, and Eu). We consider that the structural phase transitions occur in Ln_3IrO_7 (Ln= Pr, Nd, Sm, and Eu) as well as Ln_3RuO_7 (Ln= Nd, Sm, Eu, and Gd) [14–16]. In order to understand this anomaly furthermore, specific heat and DTA measurements were performed.

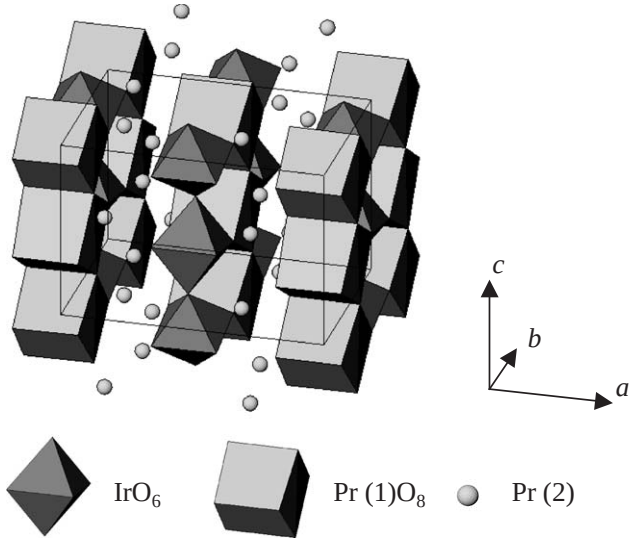

Fig. 2. Crystal structure of Pr_3IrO_7.

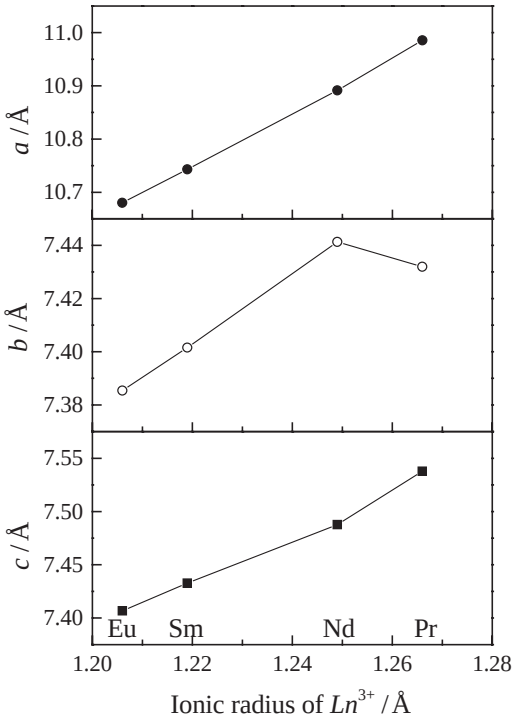

Fig. 3. Variation of lattice parameters for Ln_3IrO_7 (Ln= Pr, Nd, Sm, and Eu) with the Ln^{3+} ionic radius in eight coordination.

Figs. 4(a) and (b) show the temperature dependence of the specific heat for Pr_3IrO_7 and Nd_3IrO_7. Specific heat anomalies corresponding to the first-order phase transitions have been found at 261 K for Pr_3IrO_7 and at 342 K for Nd_3IrO_7. For Sm_3IrO_7, no such specific heat anomalies have been observed in the whole experimental temperature range. We consider that for Sm_3IrO_7 and Eu_3IrO_7, similar thermal anomalies should be observed at higher temperatures. Then the DTA measurements were performed for Sm_3IrO_7 and Eu_3IrO_7 above room temperature, and the results are shown in Fig. 5. The endothermic peaks in the DTA data during heating, which are attributable to the structural phase transition, have been found at 420 K for Sm_3IrO_7 and 485 K for Eu_3IrO_7. In order to confirm that these anomalies are due to the structural phase transitions, we performed high-temperature XRD measurements for Nd_3IrO_7 in the temperature range of 300–500 K.

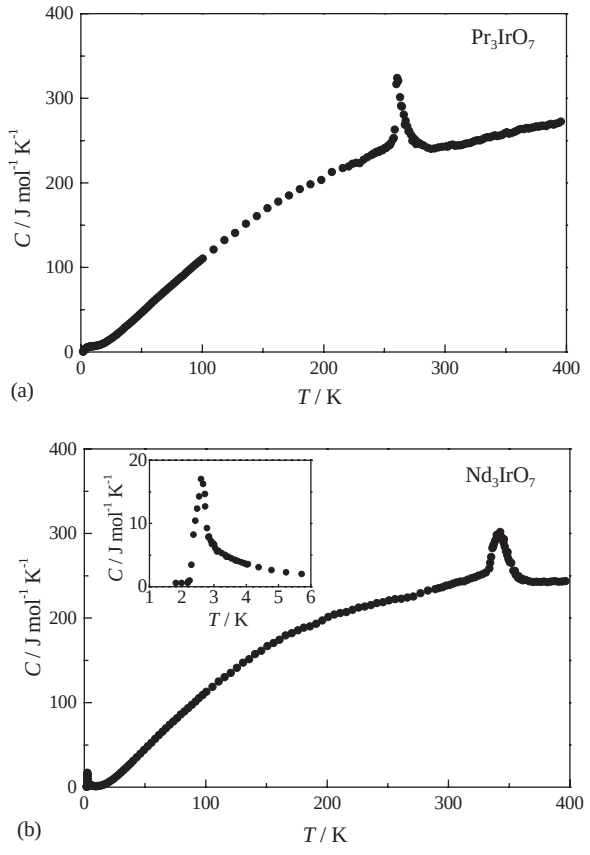

Fig. 4. Temperature dependence of the specific heat for Pr_3IrO_7 (a), and Nd_3IrO_7 (b). The inset of (b) shows the detailed temperature dependence of the specific heat for Nd_3IrO_7 below 6 K.

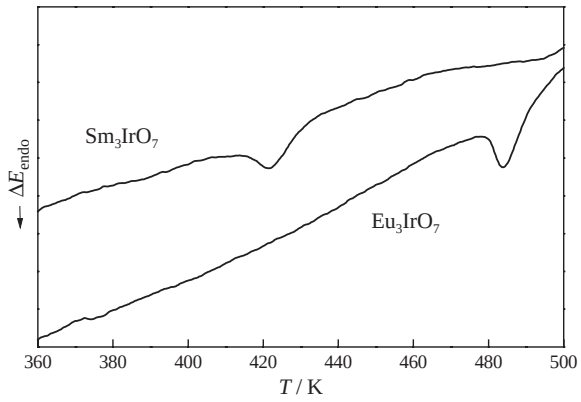

Fig. 5. DTA data for Ln_3IrO_7 (Ln= Sm and Eu) during heating in the temperature range of 360–500 K.

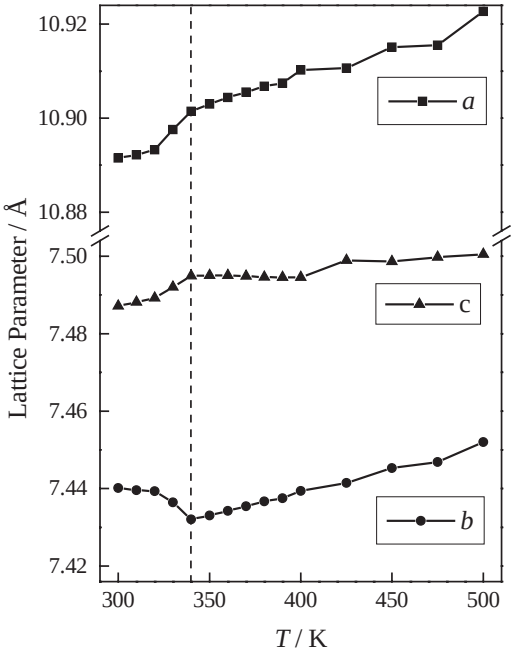

Fig. 6. Temperature dependence of lattice parameters for Nd_3IrO_7.

Fig. 6 shows the temperature dependence of the lattice parameters for Nd_3IrO_7. The lattice parameters were refined with space group *Cmcm*. They change drastically near 342 K, at which the specific heat anomaly has been observed (Fig. 4(b)). When the temperature is decreased through 342 K, the lattice parameter b is found to increase, while the lattice parameters a and c decrease rapidly. In addition, the difference is observed in the XRD profiles. Fig. 7 shows the XRD profiles measured at 300 and 350 K. The refinement for the XRD profile at 350 K was successful with space group *Cmcm*. In the XRD profile at 300 K, however, some additional diffraction lines which cannot be fitted with *Cmcm* appear at $2\theta \approx 22°$ and 25°. We consider that these extra diffraction lines originate from a low-temperature phase, and that for Nd_3IrO_7 the structure phase

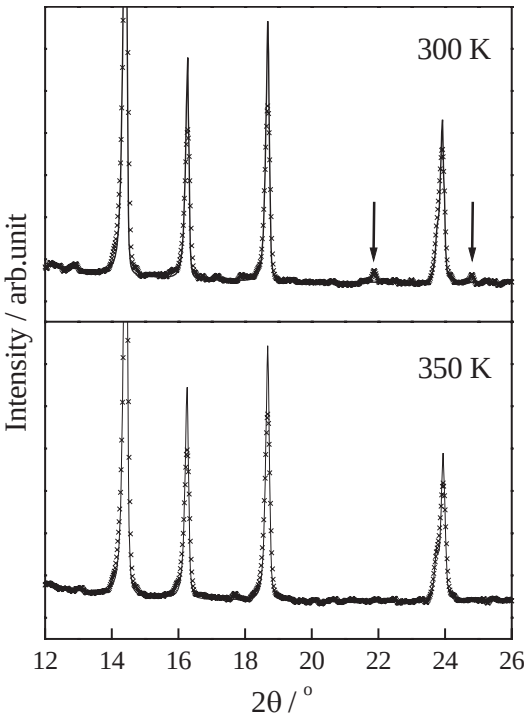

Fig. 7. Powder XRD profiles for Nd_3IrO_7 at 300 and 350 K in the 2θ range of 12–26°. Arrows show the diffraction lines which cannot be fitted with *Cmcm* (see text).

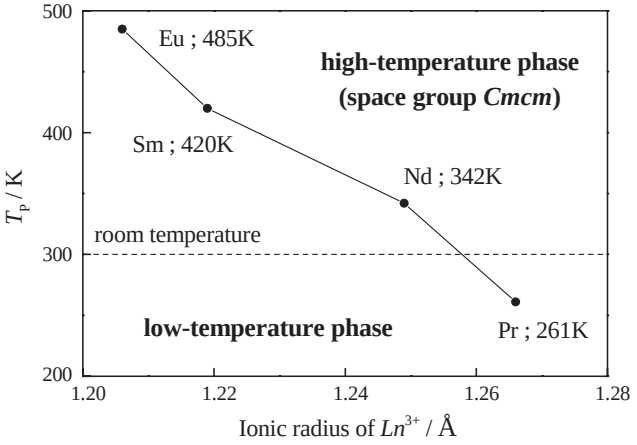

Fig. 8. Variation of the structural phase transition temperature (T_P) for Ln_3IrO_7 with the Ln^{3+} ionic radius in eight coordination.

transition occurs at 342 K. Similar extra peaks were also observed in the XRD profiles for Sm_3IrO_7 and Eu_3IrO_7 at room temperature.

The results of the specific heat, DTA and high-temperature XRD measurements indicate that the structural phase transitions occur at 261 K (Ln= Pr), 342 K (Ln= Nd), 420 K (Ln= Sm), and 485 K (Ln= Eu). Fig. 8 shows the variation of the structural phase transition temperature (T_P) for Ln_3IrO_7 (Ln= Pr, Nd, Sm, and Eu) with the Ln^{3+} ionic radius in eight

coordination. This figure shows that at room temperature only the structure of Pr_3IrO_7 is the high-temperature phase (orthorhombic, space group *Cmcm*), and those of Ln_3IrO_7 (*Ln*= Nd, Sm, and Eu) are the low-temperature phase. In other words, at room temperature the crystal structures are different between Pr_3IrO_7 and Ln_3IrO_7 (*Ln*= Nd, Sm, and Eu). This leads to the results observed in the powder XRD data (see Fig. 3). Then, we tried to determine the structure of the low-temperature phase. However, we could not obtain the detailed information on its structure from the XRD data, because the number of extra diffraction lines is limited and because their intensities are very weak. Furthermore, we performed powder ND measurements for Pr_3IrO_7 at 250 K and room temperature. The extra diffraction lines, which cannot be fitted with *Cmcm*, appear in the ND profile at 250 K. The results from ND measurements also provide the evidence that the structural phase transition occurs. We tried to determine the structure of the low-temperature phase. Unfortunately, we could not extract any valuable information to determine its structure.

3.2. Magnetic properties

Fig. 9(a) shows the temperature dependence of the magnetic susceptibility for Nd_3IrO_7 and the inset shows the detailed temperature dependences of susceptibility and specific heat in low-temperature region. An antiferromagnetic transition has been observed at 2.6 K, which corresponds to an anomaly found at the same temperature in the specific heat measurements. Nd_3NbO_7 (Nb^{5+}: diamagnetic), which is isomorphous with Nd_3IrO_7, shows the similar antiferromagnetic transitions at 2.7 K [23]. These results indicate that the antiferromagnetic transition observed in Nd_3IrO_7 is due to the magnetic interaction between Nd^{3+} ions. For all the other compounds Ln_3IrO_7 (*Ln*= Pr, Sm, and Eu), no magnetic transitions have been observed in the experimental temperature range and there is no divergence between the ZFC and FC susceptibilities. Fig. 9(b) shows the temperature dependence of the reciprocal magnetic susceptibility for Pr_3IrO_7.

In the crystal structure of Ln_3IrO_7, a pentavalent iridium ion is octahedrally coordinated by six oxygen ions. It is known that in a strong octahedral field environment, the pentavalent iridium ion has a low spin configuration ($t_{2g}^4 e_g^0$:$5d^4$) [6,24,25]. The magnetic susceptibility of such Ir^{5+} ions is independent of temperature *T* [24,25]. This causes the temperature-independent paramagnetism (TIP) term to be added to the Curie–Weiss law:

$$\chi = \frac{C}{T-\theta} + \alpha, \qquad (1)$$

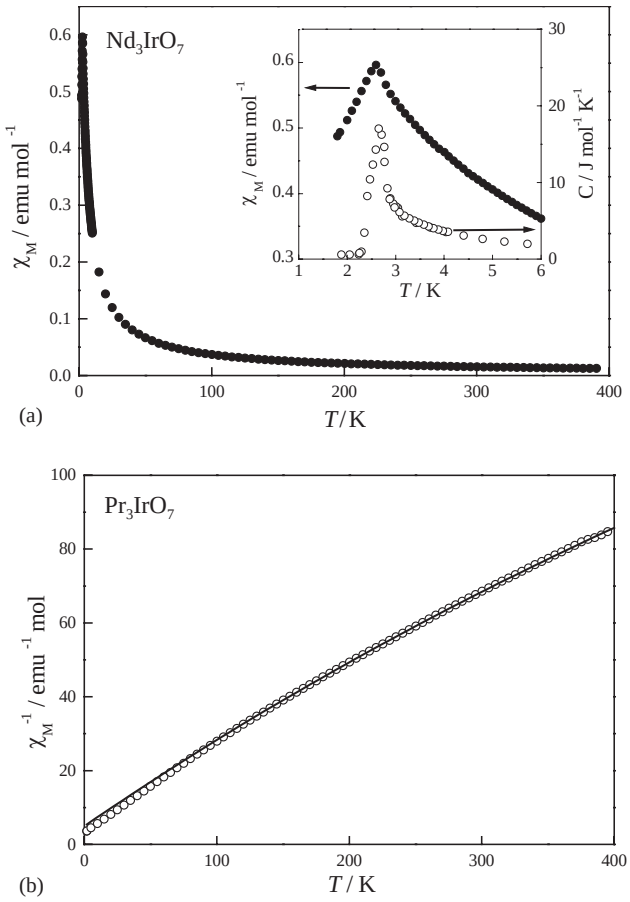

Fig. 9. (a) Temperature dependence of the magnetic susceptibility for Nd_3IrO_7. The inset shows the detailed temperature dependence of the magnetic susceptibility (filled circles) and specific heat (open circles) in the temperature range of 1.8–6 K. FC susceptibility data are not shown, because there is no divergence between ZFC and FC susceptibility data. (b) Temperature dependence of the reciprocal magnetic susceptibility for Pr_3IrO_7. The solid line shows the extended Curie–Weiss fitting with Eq. (1) (see text).

where *C* is the Curie constant (emu K mol^{-1}), θ is the Weiss constant (*K*) and α is the TIP term (emu mol^{-1}). Eq. (1), the extended Curie–Weiss law, is used for the analysis of the magnetic susceptibilities of Ln_3IrO_7 (*Ln*= Pr and Nd) and the results are listed in Table 2. The values of the effective magnetic moments for these two compounds are close to the theoretical values expected for the free Ln^{3+} ions.

4. Conclusion

Crystal structures, magnetic and thermal properties of ternary iridium oxides Ln_3IrO_7 (*Ln*= Pr, Nd, Sm, and Eu) have been investigated. The results of the specific heat, DTA, and high-temperature XRD and ND measurements show that the structural phase transitions have been observed at 261, 342, 420, and 485 K for Ln_3IrO_7 (*Ln*= Pr, Nd, Sm, and Eu), respectively. An

Table 2
The magnetic properties for Ln_3IrO_7 (Ln= Pr and Nd)

Ln	μ_{eff}/μ_B		θ (K)	α (10^{-3} emu K mol^{-1})
	Obs.	Cal.		
Pr	3.26	3.58	−20.0	2.18
Nd	3.37	3.62	−25.9	2.24

The extended Curie–Weiss fittings with Eq. (1) (see text) were performed in the temperature range of 150–260 K for Pr_3IrO_7 and 150–340 K for Nd_3IrO_7.

antiferromagnetic transition has been observed at 2.6 K for Nd_3IrO_7 from magnetic susceptibility and specific heat measurements.

References

[1] J.G. Allpress, H.J. Rossell, J. Solid State Chem. 27 (1979) 105–114.
[2] J.G. Allpress, H.J. Rossell, J. Solid State Chem. 27 (1979) 115–122.
[3] F.P.F. van Berkel, D.J.W. Ijdo, Mater. Res. Bull. 21 (1986) 1103–1106.
[4] W.A. Groen, F.P.F. van Berkel, D.J.W. Ijdo, Acta Crystallogr. C 43 (1987) 2262–2264.
[5] J.F. Vente, D.J.W. Ijdo, Mater. Res. Bull. 26 (1991) 1255–1262.
[6] J.F. Vente, Iridium-oxide compounds, Ph.D. Thesis, University of Leiden, Netherland, 1994.
[7] A. Kahn-Harari, L. Mazerolles, D. Michel, F. Robert, J. Solid State Chem. 116 (1995) 103–106.
[8] G. Wltschek, H. Paulus, I. Svoboda, H. Ehrenberg, H. Fuess, J. Solid State Chem. 125 (1996) 1–4.
[9] J.E. Greedan, N.P. Raju, A. Wegner, P. Gougeon, J. Padiou, J. Solid State Chem. 129 (1997) 320–327.
[10] P. Khalifah, R.W. Erwin, J.W. Lynn, Q. Huang, B. Batlogg, R.J. Cava, Phys. Rev. B 60 (1999) 9573–9578.
[11] P. Khalifah, Q. huang, J.W. Lynn, R.W. Erwin, R.J. Cava, Mater. Res. Bull. 35 (2000) 1–7.
[12] F. Wiss, N.P. Raju, A.S. Wills, J.E. Greedan, Int. J. Inorg. Mater. 2 (2000) 53–59.
[13] R.P. Bontchev, A.J. Jacobson, M.M. Gospodinov, V.N. Popov, B. Lorenz, R.L. Meng, A.P. Litvinchuk, M.N. Iliev, Phys. Rev. B 62 (2000) 12235–12240.
[14] D. Harada, Y. Hinatsu, J. Solid State Chem. 158 (2001) 245–253.
[15] D. Harada, Y. Hinatsu, Y. Ishii, J. Phys.: Condens. Matter 13 (2001) 10825–10836.
[16] D. Harada, Y. Hinatsu, J. Solid State Chem. 164 (2002) 163–168.
[17] R. Lam, F. Wiss, J.E. Greedan, J. Solid State Chem. 167 (2002) 182–187.
[18] J.R. Plaisier, R.J. Drost, D.J.W. Ijdo, J. Solid State Chem. 169 (2002) 189–198.
[19] R. Lam, T. Langet, J.E. Greedan, J. Solid State Chem. 171 (2003) 317–323.
[20] K. Ohoyama, T. Kanouchi, K. Nemoto, M. Ohashi, T. Kajitani, Y. Yamaguchi, Jpn. J. Appl. Phys. 37 (1998) 3319.
[21] F. Izumi, T. Ikeda, Mater. Sci. Forum 198 (2000) 321–324.
[22] R.D. Shannon, Acta Crystallogr. A 32 (1976) 751–767.
[23] H. Nishimine, Makoto Wakeshima, Yukio Hinatsu, J. Solid State Chem., in press.
[24] K. Hayashi, G. Demazeau, M. Pouchard, P. Hagenmuller, Mater. Res. Bull. 15 (1980) 461–467.
[25] M. Wakeshima, D. Harada, Y. Hinatsu, J. Alloys Compounds 287 (1999) 130–136.